Optics Communications 515 (2022) 128161

Contents lists available at ScienceDirect

Optics Communications

journal homepage: www.elsevier.com/locate/optcom

Broadband and high transmission multifunctional metasurface based on temperature-tunable InSb

Wenxuan Wu [a,b,1], Meng Zhang [a,b,1], Chengchen Wang [c], Tianyu Zhao [d,e], Nianqi Kuang [a], Youtao Zeng [a], Haixi Luo [a], Ping Jiang [a,*]

[a] College of Science, China University of Petroleum (East China), Changjiang West Road 66, Qingdao 266580, China
[b] China University of Petroleum (East China), Changjiang West Road 66, Qingdao 266580, China
[c] Tsinghua Shenzhen International Graduate School, Tsinghua University, Shenzhen 518055, China
[d] State Key Laboratory of Applied Optics, Changchun Institute of Optics, Fine Mechanics and Physics, Chinese Academy of Science, Changchun 130033, China
[e] University of Chinese Academy of Sciences, Beijing 100039, China

ARTICLE INFO

Keywords:
Temperature-tunable
Multifunctional metasurface
InSb
Anomalous refractor
Metalens
OAM beam generators

ABSTRACT

Transmissive terahertz (THz) metasurfaces have potential applications in imaging, biosensing, and optical communications. Traditional THz metasurfaces have a lot of problems such as non-adjustable spectra and low transmission efficiency. In this paper, discrete transmission phase principle and temperature-tunable material indium antimonide (InSb) are used to complete full phase coverage in the frequency range from 0.75 THz to 0.95 THz. Then a series of broadband temperature-controlled transmissive functional metasurfaces, such as anomalous refractors, focusing metalens, and orbital angular momentum (OAM) beam generators, are realized. The working states of these proposed metasurfaces can be switched from "ON" to "OFF" by adjusting the temperature of InSb from 220 K to 360 K. In addition, by adding vertical copper plates to form a Fabry–Pérot (FP) cavity-like structure, the transmission efficiencies of these metasurfaces are improved drastically to 60%. This work provides a method for designing tunable high performance multifunctional metasurface, which is expected to broaden the practical application of metasurfaces in the THz band.

1. Introduction

THz waves have many advantages such as non-ionizing radiation, high sensitivity and strong penetration, which make them have important applications in optical communications, materials science, biochemical sample identification, safety inspections, and biomedicine [1]. In recent years, the emergence of artificial electromagnetic metasurfaces in THz band has attracted widespread attention [2,3] as they can flexibly control wavefront informations of electromagnetic waves such as amplitude [4–8], polarization [9,10] and phase [11–15]. The phase modulation metasurfaces can be mainly divided into reflective-type and transmissive-type. The reflective array metasurface is a multi-layer structure composed of a planar antenna array, which is separated from the grounded metal plane by a dielectric interval of sub-wavelength thickness [16]. Some efforts have been done to design reflective broadband polarization manipulation devices [16,17]. However, the application of these reflective metasurfaces are limited as the incident wave and the output wave are on the same side, which means the incident wave will influence the performance of output wave. In order to solve this problem and meet the needs of practical applications, transmissive metasurfaces have been developed [18,19]. Zhang et al. have proposed a C-type broadband THz metalens based on the phase modulation principle of the V-shaped structure [20]. This design adopts the classic CSRR, with a phase gradient of 45°, eight transmission phase unit structures to achieve 360° full phase coverage. Pfeiffer et al. have proposed an optical four-layer cascade structure to realize full phase control and design a metalens in THz [21]. However, the efficiencies of these traditional transmittive metasurfaces are relatively low. Besides, another drawback of conventional transmittive-type metasurface is that their characteristics are difficult to adjust due to their fixed structures.

To solve these problems, we propose a InSb-based broadband transmissive temperature-tunable metasurface relying on discrete phase, which can realize different functions like anomalous refraction, focusing metalens, and OAM beam generation from 0.75 THz to 0.95 THz. The working states of these functional devices can be switched from "ON" to "OFF" successfully by tune the temperature of InSb from 220 K to 360 K. Besides, the efficiencies can be increased to 60% by applying two vertical copper layers outside the basic structure to form a F-P cavity. This work provides tunable tactic of transmittive THz metasurfaces and demonstrates a solution to improve the efficiencies, which can be

* Corresponding author.
E-mail address: pjiang@upc.edu.cn (P. Jiang).
[1] Wenxuan Wu and Meng Zhang contributed equally.

https://doi.org/10.1016/j.optcom.2022.128161
Received 7 December 2021; Received in revised form 22 February 2022; Accepted 5 March 2022
Available online 16 March 2022
0030-4018/

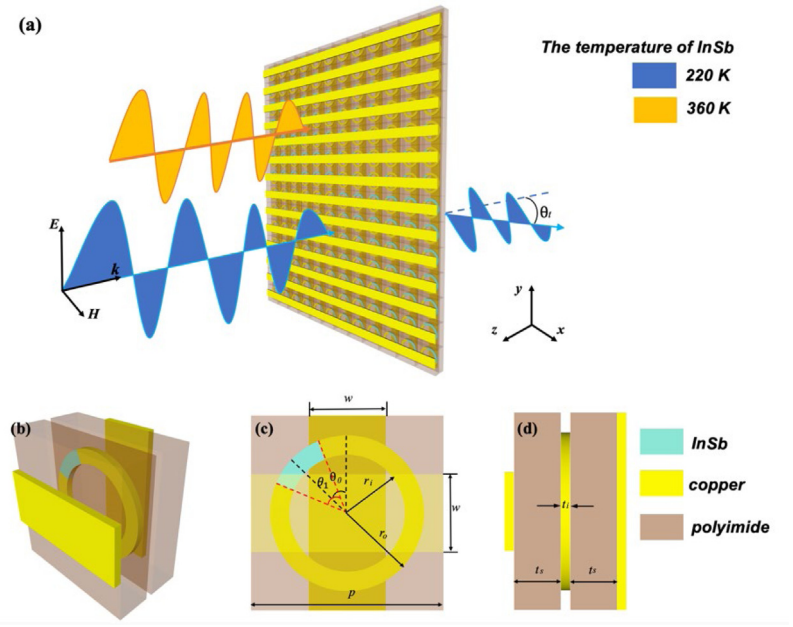

Fig. 1. (a) Schematic of a broadband transmissive temperature-tunable metasurface based on InSb, (b) The proposed meta-atom, (c) The top view of the proposed meta-atom, (d) The lateral view of the proposed meta-atom.

applied in future metasurfaces design and expand potential application of metasurfaces in imaging, communication and detection fields.

2. Structure design and theoretical analysis

Fig. 1(a) shows a schematic diagram of the broadband transmissive temperature-tunable metasurface based on InSb. And the basic meta-atom is shown in Fig. 1(b–d). The basic structure is a split copper ring, which gap is filled with InSb. Two polyimide layers are attached to the upper and lower surfaces of the ring, respectively. A couple of perpendicular copper cuboids are at the outer surfaces of the two polyimide layers separately, which can form a F-P cavity-like structure to increase the transmission efficiency. The period of the meta-atom is p, the outer radius of the copper ring is r_0, the inner radius of the copper ring is r_i, the opening angle of InSb is θ_1, the rotation direction of the copper ring is θ_0 and the thickness of the center structure is t_i. The width of the copper cuboid is w and the thickness is 5 μm. The thickness of polyimide layer is t_s. Different phase responses can be obtained by adjusting θ_0 *and* θ_1 of the structure.

The dielectric constant model of InSb can be given by the Drude model [22–27]:

$$\varepsilon(\omega) = \varepsilon_\infty - \frac{\omega_p^2}{\omega^2 + i\gamma\omega} \tag{1}$$

Where ω is the angular frequency of the incident wave, ε_∞ is the high-frequency dielectric constant, γ is the damping constant and $\omega_p = \sqrt{Ne^2/\varepsilon_0 m}$ is the plasma frequency. The relationship between the intrinsic carrier concentration N and the temperature T is:

$$N = 5.76 \times 10^{14} \sqrt{T^3} e^{\frac{-0.13}{kT}} \tag{2}$$

By the above formulas, the dielectric constant of InSb at different temperatures is simulated. It can be clearly seen that the dielectric constant of InSb is very sensitive to temperature as shown in Fig. 2. When the temperature is 220 K, the imaginary and real parts of InSb are maintained at 0 in the range of 0.75 THz to 0.95 THz, which can be regarded as an insulating material. Split rings with different opening angles can be realized. While the temperature reaches 360 K, the imaginary and real parts of InSb are similar to metal materials. Then the center structure can be seen as a close metal ring. Therefore, the proposed structure can demonstrate two different forms at 220 K and 360 K respectively.

Table 1
The relationship between θ_0 and θ_1 and the phase.

	1	2	3	4	5	6	7	8
θ_0	45°	45°	45°	45°	−45°	−45°	−45°	−45°
θ_1	23°	70°	117.5°	178.5°	23°	70°	117.5°	178.5°
Phase	0°	45°	90°	135°	180°	225°	270°	315°

Here, FDTD method is used for numerical simulations. The parameters of the proposed meta-atom are as following: p = 100 μm, r_0 = 40 μm, r_i = 30 μm, w = 40 μm, $\theta_0 = \pm 45^\circ$, t_i = 5 μm and t_s = 25 μm. By changing the opening angle of InSb θ_1 and the rotation direction of the copper ring θ_0, the eight atoms which are shown in Fig. 3(a) achieve 2π full phase coverage. And their corresponding parameters are shown in Table 1. Fig. 3(b) to (e) show the transmittances and phase shifts of the eight atoms at 220 K and 360 K, respectively. The transmission efficiency reaches over 60% in the range from 0.75 THz to 0.95 THz at 220 K. In addition, their phase shifts can achieve 0–2π full phase coverage. However, the transmittances are always below 35% at 360 K, and full phase coverage cannot be achieved. These results demonstrate that the working states of metasurfaces composed by these meta-atoms can be controlled by manipulating the temperature of InSb.

3. Multifunctional wavefront manipulation

Based on the above analysis, high transmission efficiency and full phase coverage can be achieved by adjusting the ratio of the InSb gap and the copper ring. For further research, the transmission coefficient of eight meta-atoms at 0.75 THz in Fig. 4(a) is demonstrated as well as 0.85 THz and 0.95 THz in Fig. 4(b–c). It can be clearly seen that the transmission coefficients can be changed by manipulating the temperature of InSb from 220 K to 360 K. Furthermore, it demonstrates that effect on the transmittance can be neglected by changing the operating frequency from 0.75 THz to 0.95 THz under the same temperature. These results provide a possibility to realize broadband

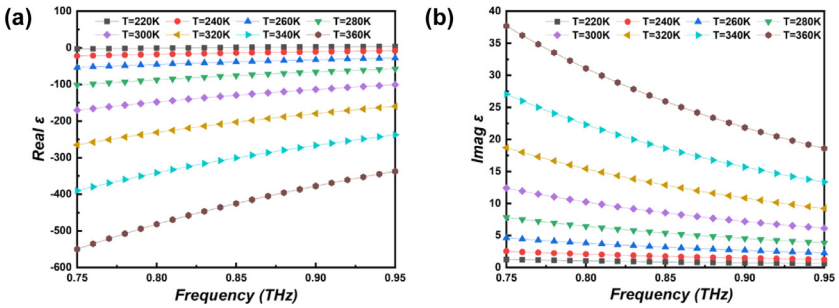

Fig. 2. The relative permittivity of InSb at different temperatures: (a) real part; (b) imaginary part.

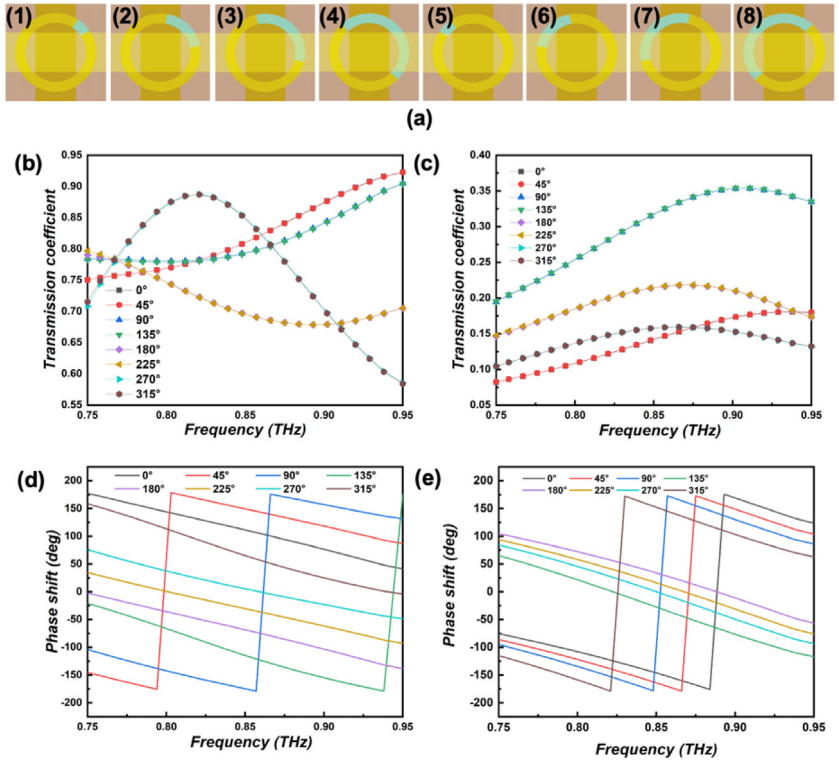

Fig. 3. (a) Schematic diagram of the supercell with 8 meta-atoms, Schematic diagram of the transmission coefficient of the proposed meta-atom at (b) 220 K (c) 360 K. And phase shift at (d) 220 K and (e) 360 K.

tunable transitive metasurfaces with phase modulation. To verify this mechanism, anomalous refractor, focusing metalens and OAM beam generator are proposed using the proposed meta-atoms.

3.1. Anomalous refractor

The deflector can control the propagation direction of the electromagnetic wave. According to the generalized refraction law, an abnormal deflection device can be designed by [28]:

$$n_t \sin\left(\theta_t\right) - n_i \sin\left(\theta_i\right) = \frac{\lambda_0}{2\pi}\frac{d\Phi}{dx} \tag{3}$$

where n_t and n_i are the refractive indices of the two media. θ_i and θ_t represent the incident angle and refraction angle, respectively. λ_0 denotes the incident wavelength in vacuum. And $d\Phi/dx$ is the phase gradient along the interface.

Therefore, according to the Eq. (3), the abnormal deflection angle at normal incidence can be calculated through the phase gradient and the wavelength of the incident light. In our research, the period of the unit structure is 100 μm, the phase gradient is $\pi/4$, the frequencies of the incident light are set as 0.75 THz, 0.85 THz, and 0.95 THz, respectively. Therefore, 8 meta-atoms as one period and we arranged three periods in a row for simulation to achieve abnormal refraction with these preset.

In order to characterize the abnormal refraction produced by the designed metasurface, the working effect diagrams of the proposed anomalous refractor at 0.75 THz, 0.85 THz, 0.95 THz are shown in Fig. 5, respectively. Fig. 5(a, d, g) show the electric fields of cross-polarized output waves at three different frequencies under the temperature of 220 K. The normally incident THz waves are deflected with refractive angles of 29°, 26° and 23°, respectively. These abnormal refraction angles of simulation results are consistent with the calculation results of formula (3). Besides, Fig. 5(b, e, h) show that the electric fields of cross-polarized output waves nearly equal to zero at three different frequencies under the temperature of 360 K, which demonstrates that the abnormal deflection does not exist. Furthermore,

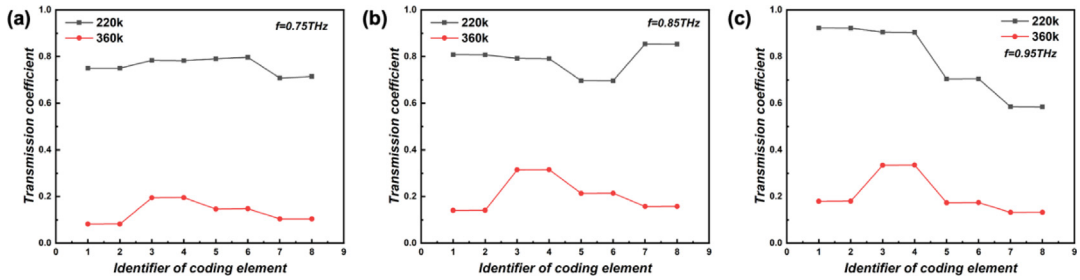

Fig. 4. The transmission coefficient of 8 meta-atoms at (a) 0.75 THz (b) 0.85 THz (c) 0.95 THz at 220 k and 360 k respectively.

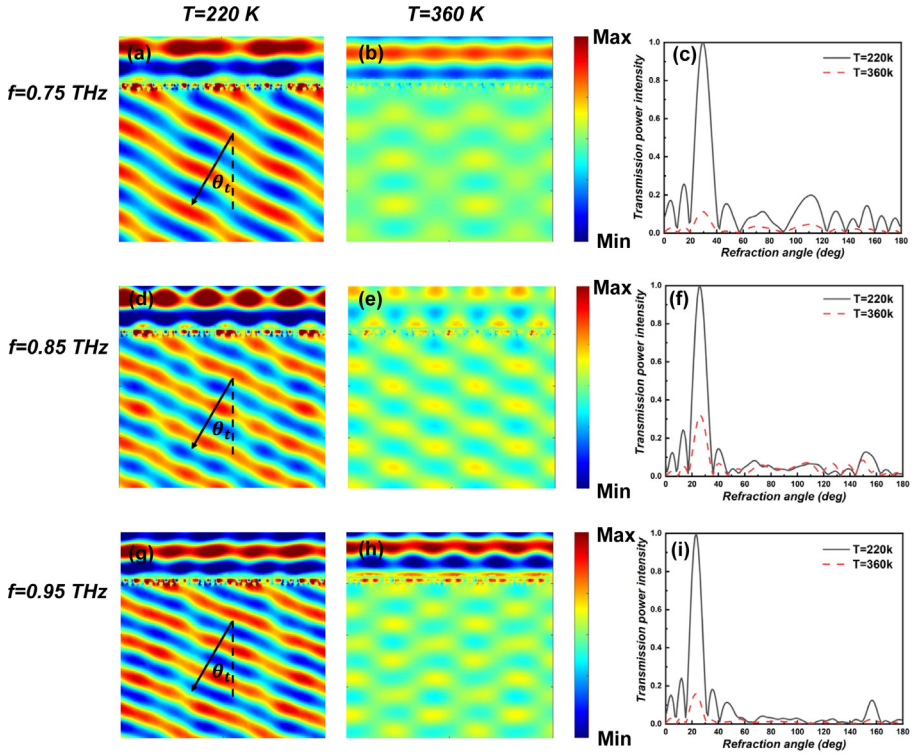

Fig. 5. The working effect diagram of the abnormal deflector at 0.75 THz, 0.85 THz and 0.95 THz at the temperature of 220 k and 360 k.

the above results can also be observed in the far-field as shown in Fig. 5(c, f, i), which also show specific transmittances at three corresponding refraction angles. It can be noted that a huge difference in transmittances between the results in 220 K (black line) and 360 K (red dash line) exists. The results illustrate that the working states of the anomalous deflector can be switched from "ON" to "OFF" by increasing the temperature from 220 K to 360 K. In addition, the proposed anomalous refractor can be worked in the frequency range from 0.75 THz to 0.95 THz successfully.

3.2. Subwavelength focusing Metalens

Metalens has the characteristics of ultra-thin, lightweight, and easy to integrate, which can make the light beams converge at a certain position by applying additional phase delay. The phase delay required for different positions is expressed by the following formula [29]:

$$\varphi(R,r) = -\frac{1}{\lambda}\left[2\pi\left(\sqrt{R^2+f^2}-f\right)\right] \quad (4)$$

Where $R = (x^2 + y^2)^{1/2}$ represents the distance from a point (x, y) to the center of the metasurface, and f represents the focal length.

Using the previously designed 8 meta-atoms, we design a metalens with a frequency of 0.85 THz and a focal length of 1500 μm. The array size of the proposed metalens is 21 × 21. Periodic boundary conditions are applied to the x and y-axes. And open boundary conditions are applied on the z-axis. The phase distribution of the metalens is shown in Fig. 6(a).

Fig. 6(c) and (d) show the intensity distribution of the transmitted electric field. It can be seen that there is an obvious convergent spot at z = 1438.77 μm at the temperature of 220 K, while the output wave cannot be converged when the temperature is 360 K. Fig. 6(b) shows the electric field intensity distribution of the x component at z = 1500 μm under the conditions of 220 K and 360 K. At the temperature of 220 K, the light intensity reaches a maximum value when x = −6.31 μm. The full width at half maximum (FWHM) of the curves is 363.30 μm, which proves that the real focal point hardly deviates from the central axis. However, when the temperature is 330 K, the intensity is only 0.24% at the focal point, indicating that the metalens does not

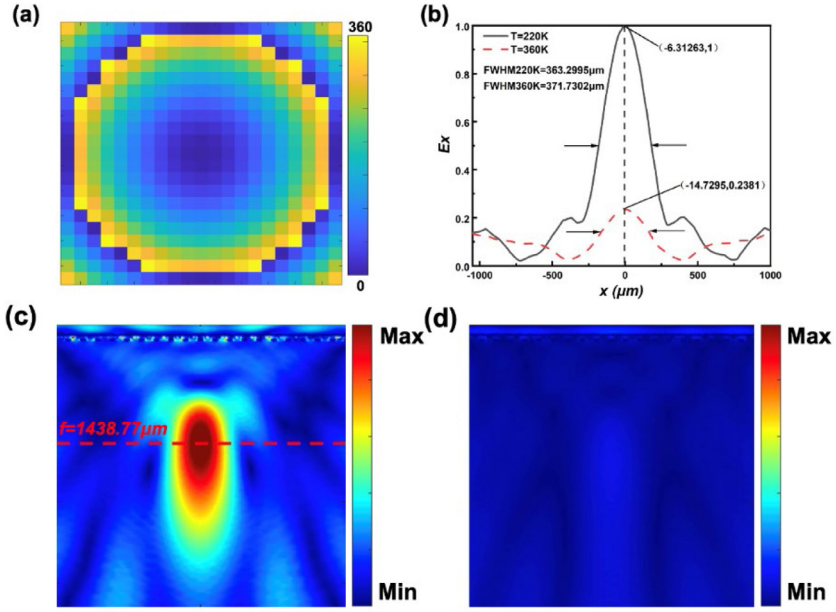

Fig. 6. (a) The phase distribution of the proposed metalens. (b) The electric field strength of the x component along x axis. (c) The intensity distribution of the transmitted electric field at 220 K. (d) The intensity distribution of the transmitted electric field intensity at 360 K.

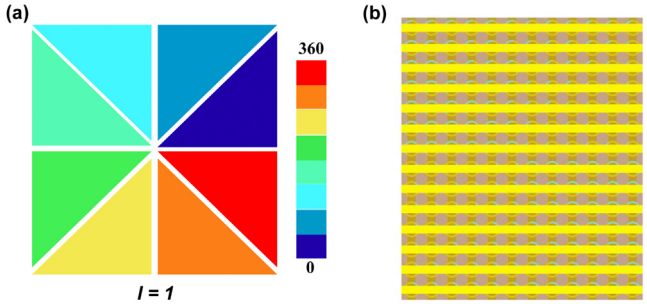

Fig. 7. Schematic diagram of (a) the topological charge of OAM beam. (b) the proposed OAM beam generator.

work under this temperature. Besides, it can also be concluded that the simulation result of the focal length (1438.77 μm) is consistent with the theoretical value of 1500 μm. These results illustrate that the working state of the focusing metalens can be adjusted by external temperature changes.

3.3. Orbital angular momentum(OAM) beam generators

Since vortex beams have unique energy distributions, OAM beam generator attract a lot of attention. In this part, we propose an OAM beam generator constructed by the proposed meta-atoms as shown in Fig. 7, of which digitized phase can be calculated in formula (5)

$$\varphi_i(x,y) = \frac{2\pi}{N} \cdot \left[\frac{l_i \cdot \tan^{-1}(y/x)}{2\pi/N} + 1 \right] \tag{5}$$

Where l represents the topological charge of OAM beam, N represents the number of regions with different phase gradients.

The topological charge is set as 1, therefore the corresponding metasurface is divided into 8 regions, which can be observed in Fig. 7. Fig. 8(a, d, g) demonstrate the phase distributions of the output wave at 0.75 THz, 0.85 THz, and 0.95 THz under the temperature of 220 K. It shows that the proposed metasurfaces can generate vortex beams at these three frequencies successfully. Besides, the corresponding mode purities at the above frequencies under 220 K are exhibited in Fig. 8(b, e, h). It shows that the purity of mode 1 is much higher than other modes at three different frequencies, which are identified with presets. As shown in Fig. 8(c, f, i), the purity of mode 1 even lower than other modes at 360 K which demonstrates that the metasurface cannot realize a preset OAM beam. These results show that the proposed OAM beam generator can be worked at 0.75 THz, 0.85 THz and 0.95 THz, respectively. And the working state can also be changed by manipulating the temperature.

4. Conclusion

In summary, we propose a thermally adjustable terahertz transmission metasurface based on InSb, which can complete the functions of anomalous refraction, focusing, and generation of vortex beam with a wide-band. Full 2π phase coverage can be obtained using the metasurface composed of the proposed meta-atoms by changing the rotation direction of the copper ring and the opening angle of InSb gap. A high transmission efficiency can reach more than 60% relying on F-P cavity-like structure. Besides, the status of these functions can be switched from "ON" to "OFF" by increasing the temperature from 220 K to 360 K due to the characteristics of InSb and they can work well in the frequency range of 0.75 THz to 0.95 THz. All the simulation results are in good agreement with the theoretical calculation results. Compared with previous work, this structure can achieve a wider spectral working range, and can achieve a controllable 60% high-efficiency through temperature regulation, which is rarely seen in previous work. The InSb-based transmissive thermally adjustable THz metasurfaces proposed in this paper exhibit advantages of thermal tuning capability, high efficiency and broadband, which are expected to expand the application range of THz wavefront manipulation.

Declaration of competing interest

The authors declare that they have no known competing financial interests or personal relationships that could have appeared to influence the work reported in this paper.

Acknowledgments

This work was funded by Central University Basic Research Fund of China (19CX02056A).

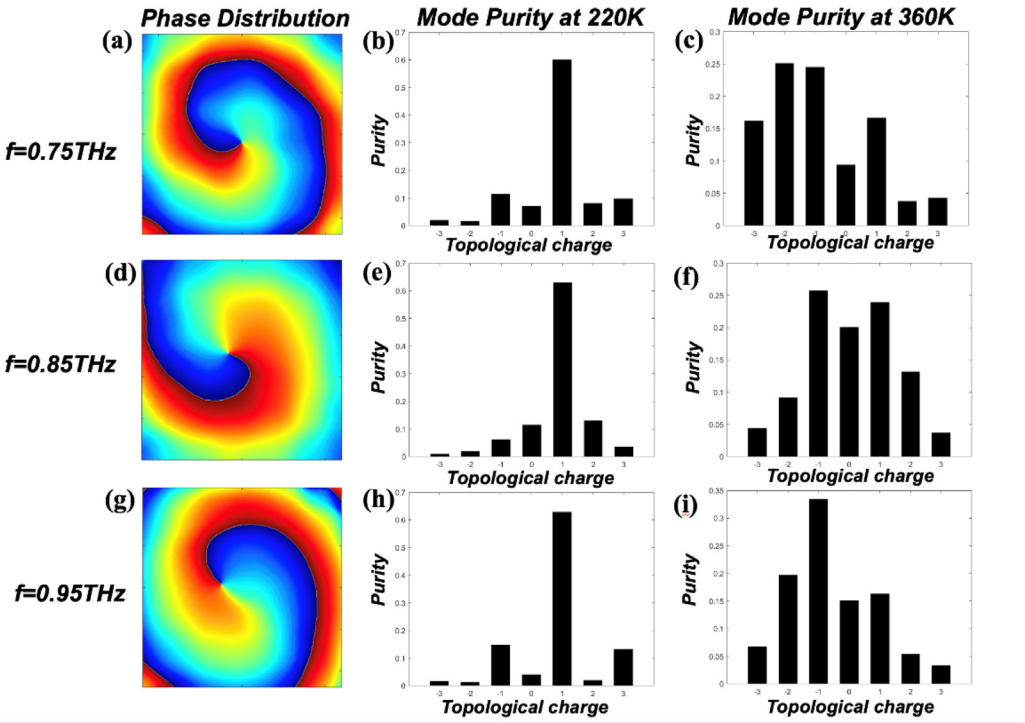

Fig. 8. Phase distributions under 220 K at (a) 0.75 THz, (d) 0.85 THz, (g) 0.95 THz. Mode purities under 220 K at (b) 0.75 THz, (e) 0.85 THz, (h) 0.95 THz. Mode purities under 360 K at (c) 0.75 THz, (f) 0.85 THz, (i) 0.95 THz.

Appendix A. Supplementary data

Supplementary material related to this article can be found online at https://doi.org/10.1016/j.optcom.2022.128161.

References

[1] Kanglin Wang, Daniel M. Mittleman, Metal wires for terahertz wave guiding, Nature 432 (7015) (2004) 376–379, http://dx.doi.org/10.1038/nature03040.

[2] R.W. Ziolkowski, E. Heyman, Wave propagation in media having negative permittivity and permeability, Phys. Rev. E 64 (5) (2001) 056625, http://dx.doi.org/10.1103/PhysRevE.64.056625.

[3] D.R. Smith, J.B. Schurig, D. Pendry, Negative refraction of modulated electromagnetic waves, Appl. Phys. Lett. 81 (15) (2002) 2713–2715, http://dx.doi.org/10.1063/1.1512828.

[4] N.K. Grady, J.E. Heyes, D.R. Chowdhury, Y. Zeng, M.T. Reiten, A.K. Azad, H.T. Chen, Terahertz metamaterials for linear polarization conversion and anomalous refraction, Science 340 (6138) (2013) 1304–1307, http://dx.doi.org/10.1126/science.1235399[10.1126/science.1235399.

[5] M. Parvinnezhad Hokmabadi, D.S. Wilbert, P. Kung, S.M. Kim, Polarization-dependent, frequency-selective THz stereometamaterial perfect absorber, Phys. Rev. Appl. 1 (4) (2014) 044003, http://dx.doi.org/10.1103/PhysRevApplied.1.044003.

[6] N.L. Mou, S.L. Sun, H.X. Dong, S.H. Dong, Q. He, L. Zhou, L. Zhang, Hybridization-induced broadband terahertz wave absorption with graphene metasurfaces, Opt. Express 26 (9) (2018) 11728–11736, http://dx.doi.org/10.1364/OE.26.011728.

[7] M. Zhang, F. Zhang, Y. Ou, J.X. Cai, H.L. Yu, Broadband terahertz absorber based on dispersion-engineered catenary coupling in dual metasurface, Nanophotonics 8 (1) (2019) 117–125, http://dx.doi.org/10.1515/nanoph-2018-0110.

[8] Z.Y. Song, J.H. Zhang, Achieving broadband absorption and polarization conversion with a vanadium dioxide metasurface in the same terahertz frequencies, Opt. Express 28 (8) (2020) 12487–12497, http://dx.doi.org/10.1364/OE.391066.

[9] Y. Zhao, M.A. Belkin, A. Alù, Twisted optical metamaterials for planarized ultrathin broadband circular polarizers, Nature Commun. 3 (1) (2012) 1–7, http://dx.doi.org/10.1038/ncomms1877.

[10] L.Q. Cong, N. Xu, J.Q. Gu, W.L. Zhang, R. Singh, Polarization control in terahertz metasurfaces with the lowest order rotational symmetry, Adv. Opt. Mater. 3 (9) (2015) 1176–1183, http://dx.doi.org/10.1002/adom.201500100.

[11] X. Yan, L.J. Liang, J. Yang, W.W. Liu, X. Ding, D.G. Xu, Y.T. Zhang, T.J. Cui, J.Q. Yao, Broadband, wide-angle, low-scattering terahertz wave by a flexible 2-bit coding metasurface, Opt. Express 23 (22) (2015) 29128–29137, http://dx.doi.org/10.1364/OE.23.029128.

[12] Z. Zhang, X. Yan, L.J. Liang, D.Q. Wei, M. Wang, Y.R. Wang, J.Q. Yao, The novel hybrid metal-graphene metasurfaces for broadband focusing and beam-steering in farfield at the terahertz frequencies, Carbon 132 (2018) 529–538, http://dx.doi.org/10.1016/j.carbon.2018.02.095.

[13] J.B. Wu, Z. Shen, S.J. Ge, B.W. Chen, Z.X. Shen, T.F. Wang, C.H. Zhang, W. Hu, K. Fan, W. Padilla, Y.Q. Lu, B.B. Jin, J. Chen, P.H. Wu, Liquid crystal programmable metasurface for terahertz beam steering, Appl. Phys. Lett. 116 (13) (2020) 131104, http://dx.doi.org/10.1063/1.5144858.

[14] Di Sha Dong, Terahertz broadband low-reflection metasurface by controlling phase distributions, Adv. Opt. Mater. 3 (10) (2015) 1405–1410, http://dx.doi.org/10.1002/adom.201500156.

[15] Y.Y. Ji, F. Fan, M. Chen, L. Yang, S.J. Chang, Terahertz artificial birefringence and tunable phase shifter based on dielectric metasurface with compound lattice, Opt. Express 25 (10) (2017) 11405–11413, http://dx.doi.org/10.1364/OE.25.011405.

[16] S. Zhang, M.H. Kim, F. Aieta, et al., High efficiency near diffraction-limited mid-infrared flat lenses based on metasurface reflectarrays, Opt. Express 24 (16) (2016) 18024–18034, http://dx.doi.org/10.1364/OE.24.018024.

[17] X. Wen, J. Zheng, Broadband THz reflective polarization rotator by multiple plasmon resonances, Opt. Express 22 (23) (2014) 28292–28300, http://dx.doi.org/10.1364/OE.22.028292.

[18] C.G. Ryan, M.R. Chaharmir, J. Shaker, J.R. Bray, Y.M. Antar, A. Ittipiboon, A wideband transmitarray using dual-resonant double square rings, IEEE Trans. Antennas Propag. 58 (5) (2010) 1486–1493, http://dx.doi.org/10.1109/TAP.2010.2044356.

[19] B. Rahmati, H. Hassani, High-efficient wideband slot transmitarray antenna, IEEE Trans. Antennas and Propagation 63 (11) (2015) 5149–5155, http://dx.doi.org/10.1109/TAP.2015.2476344.

[20] Q. Wang, X. Zhang, Y. Xu, Z. Tian, J. Gu, W. Yue, W. Zhang, A broadband metasurface-based terahertz flat-lens array, Adv. Opt. Mater. 3 (6) (2015) 779–785, http://dx.doi.org/10.1002/adom.201400557.

[21] C. Pfeiffer, A. Grbic, Cascaded metasurfaces for complete phase and polarization control, Appl. Phys. Lett. 102 (23) (2013) 231116, http://dx.doi.org/10.1063/1.4810873.

[22] R.W. Cunningham, J.B. Gruber, Intrinsic concentration and heavy-hole mass in InSb, Appl. Phys. Lett. 41 (4) (1970) 1804–1809, http://dx.doi.org/10.1063/1.1659107.

[23] S.C. Howells, L.A. Schlie, Transient terahertz reflection spectroscopy of undoped InSb from 0.1 to 1.1 THz, Appl. Phys. Lett. 69 (4) (1996) 550–552, http://dx.doi.org/10.1063/1.117783.

[24] M. Oszwalldowki, M. Zimpel, Temperature dependence of intrinsic carrier concentration and density of states effective mass of heavy holes in InSb, J.

Phys. Chem. Solids 49 (10) (1988) 1179–1185, http://dx.doi.org/10.1016/0022-3697(88)90173-4.

[25] B.S. Passmore, D.G. Vangala, W.D. Goodhure, Mid-infrared doping tunable transmission through subwavelength metal hole arrays on InSb, Opt. Express 17 (12) (2009) 10223–10230, http://dx.doi.org/10.1364/OE.17.010223.

[26] J. Manzanares-Martinez, F. Ramos-Mendieta, P. Haievi, Temperature tuning of two-dimensional photonic crystals in the presence of phonons and a plasma of electrons and holes, Phys. Rev. B 72 (3) (2005) 035336, http://dx.doi.org/10.1103/PhysRevB.72.035336.

[27] D.L. Rode, Electron transport in InSb, InAs, and InP, Phys. Rev. Lett. 3 (10) (1971) 3287, http://dx.doi.org/10.1103/PhysRevB.3.3287.

[28] N. Yu, P. Genevet, M.A. Kats, F. Aieta, J.P. Tetienne, F. Capasso, Z. Gaburro, Light propagation with phase discontinuities: generalized laws of reflection and refraction, Science 334 (6054) (2011) 333–337, http://dx.doi.org/10.1126/science.1210713.

[29] Nanfang Yu, Federico Capasso, Flat optics with designer metasurfaces, Nature Mater. 13 (2) (2014) 139–150, http://dx.doi.org/10.1038/nmat3839.